FRACTURE ENERGY OF THE CONCRETE–FRP INTERFACE IN STRENGTHENED BEAMS

Mithila Achintha and Chris Burgoyne

Biography: Mithila Achintha is a post-doctoral researcher at the University of Oxford, UK. He received his BSc(Eng) from University of Moratuwa, Sri Lanka; and PhD from University of Cambridge, UK; in 2003 and 2010 respectively. His research interests include the application of FRPs in civil engineering and fracture mechanics of concrete.

Chris J. Burgoyne is Reader in Concrete Structures at the University of Cambridge, UK. He is a member of ACI Committee 440. His research interests include advanced composites applied to concrete structures.

ABSTRACT

To determine the load at which FRPs debond from concrete beams using global-energy-balance-based fracture mechanics concepts, the single most important parameter is the fracture energy of the concrete–FRP interface, which is easy to define but difficult to determine. Debonding propagates in the narrow zone of concrete, between the FRP and the (tension) steel reinforcement bars in the beam, and the presence of nearby steel bars prevents the fracture process zone, which in concrete is normally extensive, from developing fully. The paper presents a detailed discussion of the mechanism of the FRP debonding, and shows that the initiation of debonding can be regarded as a Mode I (tensile) fracture in concrete, despite being loaded primarily in shear. It is shown that the incorporation of this fracture energy in the debonding model developed by the authors, details of which are presented elsewhere, gives predictions that match the test results reported in the literature.

Keywords: concrete–FRP interface, debonding, fracture energy, Mode I fracture, mixed-mode loading, strengthened beam

INTRODUCTION

This paper addresses one particular topic that is important in the analysis of the debonding of FRP plates from concrete beams, and forms part of a much larger study[1-3]: only a brief outline of which is given here. That work has been validated against many experiments carried out by others, requiring knowledge of the fracture energy of concrete; this is not a parameter that is normally measured when performing experiments. This paper explains why particular values for the fracture energy of concrete have been used in the larger study.

Premature FRP debonding hampers efficient use of externally bonded FRP plates in flexural strengthening of concrete beams, and uncertainty about the governing mechanisms means that there is no reliable theory that can be applied by designers. Debonding initiates from the propagation of a dominant crack in the vicinity of the concrete–FRP interface, and hence fracture-mechanics-based finite element (FE) approaches have often been used in the literature to determine failure load[4]. These fracture analyses were often based on the pioneering theories of Hutchinson and Suo[5], which were intended for the analysis of interface debonding in thin-layered elastic materials. However, in contrast to materials like glass, it is generally assumed that the fracture process zone (FPZ) in concrete is large, typically over 12 in. (300 mm) long with a width of several times the aggregate size[6]. As a result, the concrete–FRP interface cannot be modeled using the concepts of linear elastic fracture mechanics (LEFM). Nonlinear FE models, such as the J-integral technique that would be needed to simulate FRP debonding, require far more detail of the interface properties (such as the distribution of voids in the interface between the adhesive and the concrete, and

knowledge of the aggregate distribution) than will ever be available, even to the analyst of laboratory experiments, and certainly not to designers. It should be noted that, despite FE analyses being capable of providing accurate solutions for complex structural mechanics problems such as fracture in metals, the technique is not proven as a reliable tool for analyses of concrete structures[7]. In FE simulations, the crack path must be known *a priori*; a crack follows the path of least resistance around or through the aggregate, but reliable estimates for relative fracture resistances of aggregates and the interface between aggregate/cement-paste cannot be made. Alternatively, the use of smeared-crack FE models avoids the need to model discrete cracks, but this approach fails to model debonding, which is triggered by the propagation of a dominant single crack. Moreover, very small elements (typically, with dimensions < 0.04 in (1 mm)) are needed in FE simulations to obtain consistent results for fracture parameters. At this length scale, concrete does not behave as a homogeneous material. As a further complication in the analysis of FRP debonding, the effect of the steel bars present in the FPZ (**Fig. 1**) is difficult to model. The effect of the steel bars on the FPZ may be incorporated in the FE simulations by imposing a boundary condition in the form of a known strain but no accepted method exists in the literature.

A high stress may cause a crack to form near the interface, but that crack will only propagate if more energy is thereby released than it takes to form the new fracture surfaces. It is thus a fracture mechanics problem so an accurate solution cannot be determined from methods based on a detailed stress analysis. In recently developed non-linear fracture mechanics models[8], the results of shear-lap tests were used to derive the fracture parameters that govern FRP debonding. However, as is shown below, these tests do not provide accurate fracture parameters that can be used in the analysis because of the difference between the mode of fracture that takes place in strengthened beams and that in a shear-lap test. In addition, the

FRP carries a very high tension force (F_p), acting at an eccentricity with respect to the tip of the shear/flexural crack that forms the critical interface crack. This introduces a significant tension at the crack tip causing a tensile fracture; none of the reported studies take account of this effect. As an alternative, Oehlers et al. (2011)[9] recently presented a model, based on the rigid-body rotations that take place at the dominant flexural crack that triggers debonding. This model, however, requires precise details of the crack locations and only considers the effect of a single flexural crack in the beam. Although a number of models have been reported, none of this provides a comprehensive tool to analyse FRP debonding.

The present authors have earlier developed a global-energy-balance-based fracture mechanics model for the analysis of FRP debonding[1-3]. The model obviates the need for FE analyses. The model assumes that flaws are inevitable in the interface, and predicts that debonding will occur when the energy available to drive a small extension of an existing interface crack exceeds the energy needed to form the new fracture surfaces. Two key governing parameters are compared in the model to determine debonding: the energy release rate (i.e. the energy release due to a unit extension of a crack of unit width $-G_R$) and the interface fracture energy (the energy required to form new fracture surfaces needed to accommodate a unit extension of a crack of unit width$-G_{F_int}$). Manufacturers have now developed sufficiently tough adhesives that, if used correctly, failure usually takes place in the concrete just above the interface (**Fig. 1**). Thus, it is possible to assume that G_{F_int} is the same as the fracture energy of concrete (G_C). The *critical crack* – i.e. the smallest crack that can propagate rapidly under the given conditions – can be determined when $G_R = G_C$. Thus, for a given beam, the model can determine either the crack length that triggers failure at the design load, or the failure load of a beam with an existing crack of known length. The model predictions, based on this concept adopted in the analyses, matched well with test data reported in the literature[3].

When the fracture occurs, the beam loses some of its stiffness, so work is done by the external loads. The curvature increases in the beam, storing some of this extra work as strain energy, but some is left over to cause the crack to propagate. The G_R during fracture extension can be determined if the energy states of the beam before and after the crack extension are known[1,2]. An accurate analysis of the energy state of a beam using its stress–strain variations over the whole span is very complex, so a simpler integration of moment–curvature (M–κ) was used, but even determining the curvature is complex[1]. A modified form of Branson's model, which determines the M–κ relations and hence the energy state of a beam was developed; this analysis is presented elsewhere[1,2].

If the technique of flexural strengthening of beams is to be useful, it is necessary to know the G_C of the concrete from which the beam is made. But G_C is not a property that can be determined reliably, either theoretically or experimentally, even in a research context. To determine G_C theoretically, knowledge of the stress–displacement relations in the FPZ are required, and it is more accurate to rely on experimental investigations. However, inconsistent fracture data can result from experiments since the FPZ may not develop fully in the small specimens usually used in tests. Also, interface debonding is caused by a combination of normal and shear stresses[2], and determination of this fracture energy is very complicated. It is virtually impossible to set up experiments to simulate the actual mixed-mode loading conditions present in the interface of strengthened beams.

This paper raises a number of issues that are controversial, and go against accepted wisdom; the logic will be explained in more detail below.

- Conventional fracture analysis would fail to determine the G_C in the vicinity of the interface, because the FPZ cannot develop fully due to the presence of the steel bars.

- FRP debonding from concrete beams can be regarded as a Mode I fracture in concrete, which explains why the shear-lap experiments often used in the literature do not provide results that are useful. Instead, it is necessary to use data from experiments designed to determine the tensile fracture energy. The paper shows how the fracture energies of the beams quoted in the earlier papers by the authors[3] were determined.
- The fracture energy can be regarded as independent of the length of the debonding crack, even though the FPZ cannot develop fully, because the strain conditions near the tip of the crack remain unchanged as the crack develops.
- The data provided by this analysis can predict debonding loads in a range of strengthened beams that have been reported in the literature.

RESEARCH SIGNIFICANCE

The paper argues that debonding failure of FRP-strengthened beams takes place by a tensile (Model I) fracture of the concrete in the cover zone of the beam. The presence of the steel bars nearby limits the extent to which the FPZ can develop, and means that the fracture energy is independent of the length of the existing crack. This is of fundamental importance for the use of fracture mechanics in the analyses of FRP debonding from concrete beams.

MECHANISM OF FRP DEBONDING

The plate end, and zones where widening of flexural cracks cause interface flaws, are most susceptible to the initiation of debonding; the two modes are referred to as "plate-end" (PE) and "intermediate-crack-induced" (IC) debonding respectively (**Fig. 2**).[2] PE debonding initiates at the vicinity of the FRP end and propagates towards the middle of the beam, whereas IC debonding initiates at a high-moment zone and propagates towards a low-moment zone. In both modes, fractures propagate in the concrete substrate between the FRP and the

tension steels of the beam[4]. Usually, the whole concrete cover of the beam separates during PE debonding, and only a few millimeters thick concrete layer separates during IC debonding.

Interfacial stress concentrations

A crack in a material can propagate either by opening (Mode I), shearing between the two crack faces (Mode II), or by a combination of both (mixed-mode). In different modes of fracture, different stress–displacement fields will develop in the vicinity of the crack, so the fracture energy depends on which fracture mode occurs. Although cracks in brittle, isotropic, homogeneous solids propagate by maintaining pure Mode I condition at the crack tip, the stress field that triggers debonding at an interface can be very complex[5]. Various forms of stress concentrations develop due to the different fracture toughnesses of the two joining materials and also there are a number of geometric constraints[5].

Plate-end (PE) debonding

If the FRP plate is curtailed at a considerable distance away from the beam support, a dominant shear crack can be formed in the concrete beam near the plate end [2]. There are two mechanisms that may cause the crack to propagate towards the beam along a direction about 45º to the interface (**Fig. 3a**). The FRP force acts at an eccentricity with respect to the tip of this shear crack, where it induces significant tension (**Fig. 3a**). The crack will propagate by opening of the crack tip in the direction perpendicular to that of the maximum principal tensile stress (MPTS). The relative vertical displacements between the two crack faces of the original shear crack can also contribute to the propagation of the crack towards the beam.

Various other mechanisms can also introduce additional interfacial stress concentrations, which will contribute to the further propagation of the original crack. The concrete beam is

very stiff by comparison with the FRP, so the beam remains effectively straight, while the eccentricity between the tension in the FRP and the concrete surface tends to peels away the FRP from the beam. Moreover, the axial strain of the bonded FRP is zero at its ends, but since the FRP is curtailed at a nonzero moment location, the adjacent surface of concrete has a nonzero axial strain. The full strain compatibility between the beam and the FRP is only satisfied some distance away from the FRP end. The stress gain in the FRP at its end is very rapid and is associated with a development of significant interfacial shear stresses. These interfacial stress concentrations cause the development of the original shear crack, however because of the presence of the steel bars, rapid propagation of PE debonding usually takes place at the level of the steel, separating the entire concrete cover from the beam.

Intermediate-crack-induced (IC) debonding

The relative sliding between the two faces of a flexural crack in a high moment zone of the beam forms interface flaws, and these movements of the crack faces will also introduce the peeling force that is required to trigger debonding (**Fig. 3b**). In addition, the transfer of tensile stresses from the concrete to the FRP at the crack location introduces high interfacial shear stresses. If the stress concentrations that develop at the interface crack exceed the critical state, debonding takes place towards a low moment zone of the beam (**Fig. 2**). Note that, since the principal stress would be at about 45º to the interface, it is expected that the crack would move into the beam. However, this will not happen since a high F_p acts eccentrically to the crack tip, taking the fracture back down towards the interface (**Fig. 3a**). Thus, only a thin layer of concrete separates here, in comparison to that during PE debonding.

A complex stress field that develops in the vicinity of a critical interface crack triggers debonding. G_C of concrete against mixed-mode loading is therefore needed to determine the

loads at which debonding occurs, although it will be contended below that the Mode I effects dominate the propagation of debonding. Note that it is virtually impossible to accurately determine these stress fields and therefore any method that purports to compare predicted detailed stresses with interface strength is almost guaranteed not to provide a reliable solution.

FRACTURE ENERGY OF CONCRETE UNDER MIXED–MODE LOADING

A crack under mixed–mode loading can experience either kinking or straight-ahead propagation, depending on the relative fracture resistances associated with the competing possible directions of advance[5]. The mixed-mode fracture energy ($G_{CI/II}$) thus depends on the magnitude of the component of each primary mode of fracture involved during a unit total extension of the crack and the also on the respective fracture energies of pure primary modes (i.e. G_{CI} and G_{CII} respectively) (Eq. [1])[5]. The relative contributions of each primary mode (i.e. the mode mixity–ψ), is defined as the ratio of the components of Mode II to Mode I. $G_{CI/II}$ usually increases with the increase of ψ since G_{CII} is often higher than G_{CI}.

$$G_{CI/II} = (1-\psi)G_{CI} + \psi G_{CII} \qquad [1]$$

Mechanism and fracture energy of Mode I crack

Under uniaxial tension, when the applied stress at the tip of an existing traction-free crack reaches the tensile strength (f_t), the crack starts to open in the direction perpendicular to that of the stress. A new portion of the crack is formed in front of the crack tip, and thus, the crack starts to propagate by opening (i.e. Mode I crack) (**Fig. 4a**). However, until the tip of the original traction-free crack (Point A in **Fig. 4a**) opens up to a certain critical value (w_c), stresses continue to transfer across the newly-formed part of the crack faces, since the aggregate pieces "bridge" the crack. Once the crack has opened beyond w_c, the newly-formed crack faces become traction-free. The energy required to open the new part of the crack faces

from its initial intact state to the current traction-free state is $G_{C\mathrm{I}}$. Thus, $G_{C\mathrm{I}}$ of a concrete depends on the magnitudes of both f_t and w_c. Typically, f_t<0.73 ksi (5 N/mm^2) and w_c < 0.008 in. (0.2 mm)[11] which results in a relatively low $G_{C\mathrm{I}}$ (usually, $G_{C\mathrm{I}}$ < 0.86 lbf/in. (0.15 N/mm)).

Mechanism and fracture energy of Mode II fracture

To propagate a crack in shear, the two crack surfaces need to displace relative to each other over the whole length of the fracture plane (**Fig. 4b**). Therefore, large crack plane separations, of the same order of magnitude as the size of the aggregate, are required to propagate a Mode II crack in concrete. A Mode II crack follows a tortuous path and propagates against high friction/aggregate interlock resistances in comparison to the much lower $G_{C\mathrm{I}}$, where crack plane separations of less than 0.008 in. (0.2 mm) is required to drive a crack. As expected, the $G_{C\mathrm{II}}$ values reported in the literature are significantly higher than $G_{C\mathrm{I}}$ (often more than 20 times)[12]. There is also a large scatter in the reported $G_{C\mathrm{II}}$ values which may be attributed to the different effective fracture areas experienced in different test specimens.

Local Mode I crack extension under mixed-mode loading

Because of the relatively high shear fracture resistance of concrete, it has been widely assumed that a crack under mixed-mode loadings propagates by opening of the crack tip, although the direction of propagation depends on the mode mixity[12]. It has been further assumed that a crack starts to open when the MPTS at the crack tip reaches f_t, and the instantaneous propagation will be in the direction perpendicular to that of the MPTS [12]. Thus, it is appropriate to assume that the crack opening will be associated with the same fracture energy as that under pure Mode I. This assumption has been widely validated in the literature[12]; the test results for the fracture paths matched well with that obtained from FE simulations based on the MPTS failure criterion with $G_{C\mathrm{I}}$ as the governing parameter. Note

that those FE analyses would not have been affected by non-linear material behaviour because of the very low working strains, and also the fact that the test specimens should have been free from cracks other than the one where propagation was studied.

MODE I FRACTURE ENERGY OF THE CONCRETE–FRP INTERFACE

It has been assumed here that, irrespective of the mode mixity, a crack in concrete will grow locally by opening in the direction perpendicular to MPTS. In this way, an interface of a strengthened beam, which is primarily carrying shear, actually fails in tension. In PE debonding, the F_p acts eccentrically to the tip of the shear crack that triggers debonding, causing a moment that causes dominant tension in the crack tip, and hence the crack propagates by opening of the crack tip (**Fig. 3a**). Thus, instantaneous propagation of PE debonding takes place as a Mode I fracture in concrete. During IC debonding, there is no moment induced by the FRP, which remains attached to the concrete at both ends of the unbonded zone. However, this attachment means that only infinitesimal sliding can take place and the large fracture energy associated with Mode II fracture cannot be developed. However, because the FRP is so thin, it is relatively easy for it to move slightly away from the concrete surface, thus mobilizing the much lower Mode I fracture energy.

Bond-slip models

Single/double-shear-lap experiments (**Fig. 5a**) have commonly been used[13] to determine the parameters for the analysis of FRP debonding. The specimens failed due to shear fractures that occurred within the concrete substrate, adjacent to the concrete–FRP interface. The maximum shear stress that can be resisted by the interface and the fracture energy were usually determined using the bond–slip relationships measured in the tests. In a shear–lap test, the concrete substrate fails in shear whereas it is asserted here that a Mode I fracture

triggers FRP debonding from concrete beams. Therefore, it is contended that these tests do not provide meaningful fracture parameters that can be used in the analysis of FRP debonding. Fracture energy values derived from a shear–lap experiment (i.e. G_{CII}) will be significantly higher than that against debonding of FRPs in strengthened beams, and they also depend in a complex way on the area of the fracture plane that has been formed in the experiment. Tests with different widths of FRPs on identical concrete blocks resulted in different fracture energies[13]. A few recent studies[8], have used the bond-slip results derived from shear-lap experiments, in smeared-crack based FE models to analyse FRP debonding. The selection of Mode II fracture parameters in these models, however, does not represent the actual mechanism of FRP debonding where a Mode I fracture triggers fracture.

Some recent research studies have experimentally investigated the Mode I fracture energy in the vicinity of concrete–FRP interface[14], although the tests were not aimed modelling FRP debonding as a Mode I fracture of concrete. Qiao and Xu[14] used a modified three–point bend specimen, where the specimen was made by joining two halves of the beam, one having an epoxy bonded FRP and the other an adhesive layer on the joining surfaces (**Fig. 5b**). A Mode I fracture was observed, within the concrete substrate at one side of the beam, but close to the interface. The fracture energy calculated from that study[14] is of similar magnitude to that of pure concrete (0.6–0.9 lbf/in.(0.1–0.15 N/mm)). Thus, if the failure takes place within the concrete, the presence of nearby FRP does not affect G_{CI}.

INVARIANCE OF THE FRACTURE ENERGY IN FRP DEBONDING

When a fracture develops in a large block of concrete, it is possible for the FPZ to fully develop. The energy required to extend the crack can thus be expected to vary as the crack gets longer; that variation is referred to in fracture mechanics literature as the R-curve.

Although R–curve analyses of some non-linear materials, such as steel and FRP composites, are now well established, no accepted data exists for concrete.

Although a few studies, such as the equivalent-LEFM-based model of Shah and Ouyang[15] have been reported, no conclusions were drawn. During a test, it is difficult to identify the FPZ when the crack has just formed, while the existence of a large FPZ means the results are influenced by the geometry of the test specimens. Despite considerable research during the 1980s, there has been very little work recently on the R–curve of concrete. No advances over earlier understanding have been observed, even in the limited recent studies[16]. Even for cement paste, which has a much simpler microstructure, there is no consistent data.

Fig. 6 shows a crack forming in the cover zone between the FRP and the steel reinforcement; two positions are shown, one before and one after the crack has extended. Both the steel and the FRP are bonded to the concrete ahead of the crack, so the strain in the concrete is limited. The effect is that the FPZ is of limited extent. Furthermore, the FPZ cannot be influenced by the length of the crack, because it is not possible for any deformation of the FRP (the concrete being sensibly rigid) to change the state ahead of the crack tip. Thus, the FPZ ahead of the crack tip in State 2 is of the same extent as it was in State 1. If the FPZ is the same, the fracture energies must be independent of the length of the crack.

The corollary of this argument is that the fracture energy to be used in a debonding analysis should be the value obtained from small-scale test specimens, or from the initial stages of tests on larger specimens when the crack has not fully developed. This is consistent with earlier analyses of FRP debonding[3] that have shown that interface cracks of about 0.8–1.2 in. (20–30 mm) and 0.1–0.2 in. (2–5 mm) long cause PE and IC debonding respectively.

DETERMINATION OF THE MODE I FRACTURE ENERGY OF CONCRETE

Knowledge of the stress vs. crack-opening (σ–w) relationships in the FPZ, during a unit extension of a Mode I crack, is required to determine G_{CI}. However, this analysis is not trivial since the σ–w relationships of concrete depend on many microstructural features which are unknowable. No accepted method is reported in the literature for this analysis, and therefore, it is more accurate to determine G_{CI} of a given concrete using experiments.

Experimental evaluation of G_{CI}

Standard methods[17] based on energy balance during the experiments of notched–beam specimens, together with appropriate correction factors to take account of the effects due to small test specimens, are now well established to determine G_{CI} . As confirmed by recent studies[16], these experiments can be used to obtain reliable estimates for G_{CI} . Note that inaccurate G_{CI} evaluations have been made, and are still being made, based on an empirical formula quoted in the CEB–FIP model code[11], which is simple to use, because it is based on the compressive strength ($f_c^{/}$) and the maximum size of the aggregates (d_a) of the concrete. However, this formula was based on an earlier RILEM report[18] that recommends the direct estimation of G_{CI} from the results of beam specimens without taking account of the size effect of concrete; thus, the method underestimates G_{CI} in most cases.

Simplified approximate models for G_{CI}

Although it is possible to obtain reliable estimates for G_{CI} from tests, the experimental investigations are not trivial and are often associated with several practical and conceptual difficulties. A stiff testing machine is needed to allow stable fractures in concrete. Simplified models, albeit approximate, which are usually presented in terms of more readily known properties of concrete such as $f_c^{/}$ and d_a, are useful to determine G_{CI} .

The cohesive crack model

The cohesive crack model[19], which models the development of the FPZ by the stress vs. crack-opening relationship at the tip of a traction-free crack, is widely believed to be the best performing fracture model for concrete and is widely used in the fracture analysis of concrete. The model is also very useful in the experimental studies since only the characteristics at the original crack tip, whose geometric location is precisely known, need to be studied.

A traction-free crack is assumed to open when stress at the crack tip (σ_{tip}) reaches f_t. Thus, at the crack tip (Point A in **Fig. 7**), a zero crack opening is associated with a σ_{tip} of f_t. The widening of the crack tip (w_{tip}) causes the crack to propagate. However, the aggregate pieces bridge the crack and hence there will only be a gradual decrease in σ_{tip} to zero as w_{tip} grows to a critical value (w_{tip_c}) where there is no stress transfer between the crack surfaces in the FPZ. The σ_{tip}–w_{tip} relation is referred to as the tension-softening response, and it is assumed that the part of the crack opening where $w_{tip}<w_{tip\_c}$ characterises the development of the FPZ. The area under the σ_{tip}–w_{tip} curve (**Fig. 7**) – i.e. work done against cohesive forces present in the FPZ (Eq. 2) – represents G_{CI}. The model thus provides an alternative way to estimate G_{CI}, avoiding the need for knowledge of the stress–crack opening relations in the FPZ.

$$\int_0^{w_{tip\_c}} \sigma_{tip}\, dw_{tip} = G_{CI} \qquad [2]$$

Tensile strength and the tension-softening response

The tensile strength (f_t) and the tension-softening response are both required to determine G_{CI}.

Tensile strength

The f_t of a concrete can be influenced by the heterogeneity of the mix and also the type of stress field that causes the failure. However, it is generally assumed to have a known relation to the f_c' of the mix; the EuroCode 2[20] recommendation is used in the present work (Eq. 3).

$$f_t = 0.158(f_c')^{2/3} \text{ ksi} \qquad (f_t = 0.30(f_c')^{2/3} \text{ N/mm}^2) \qquad [3]$$

Determination of the tension-softening response

In the reported experiments[21], uniaxial tensile tests were carried out using very stiff testing machines. However, the location of the fracture is not known *a priori*, so study of the critical zone prior to development of significant microcracks is very difficult. A notched specimen helps to identify the critical zone, but the notch introduces additional stress concentration. The tests assume a uniform stress distribution across the specimen, but once the fracture has initiated a significant stress gradient will develop near the crack.

Despite it being virtually impossible to obtain precise results for the exact σ–*w* relationships, the experiments are capable of providing the approximate shape of the softening curve. This can then be adjusted until the area under the softening curve equals the independently determined more reliable estimate of G_{CI}. This allows the correlation of the softening response with more readily-known properties of concrete such as f_c' and d_a. The simplified models can then be used for the estimation of G_{CI} of other concretes.

Simplified tension-softening models

A rapid development of microcracks followed by stable widening of a critical macrocrack is observed in the tests[22]. Thus, the shape of the softening curve has been approximated by using bilinear[22] and polynomial[23] models with f_t and w_{tip_c} as the key parameters (**Fig. 8**).

Bilinear models

In bilinear models, the coordinates of the kinking point (f_1, w_1), and w_{tip_c} are required to determine G_{CI} (**Fig. 8a**). It has been reported that f_1 is about 1/3 of f_t [22], and a range of values between 0.001–0.0015 in. (0.03–0.04 mm) were quoted for w_1 [21,22]; these values are assumed

in the present study. The stress transfers between the crack surfaces, and hence, w_{tip_c}, depend upon d_a of the mix. The CEB–FIP model code[11] recommends typical w_{tip_c} values of 0.005, 0.006 and 0.01 in. (0.12, 0.15 and 0.25 mm) for concretes with crushed aggregate of 0.3, 0.6 and 1.3 in. (8, 16 and 32 mm) respectively. In the present study, these values are assumed with appropriate interpolations to determine w_{tip_c} of concretes with other sizes of aggregate.

Polynomial models

The power relation developed by Reinhardt[23] is the most widely quoted model in the studies.

$$\sigma = f_t \left[1 - \left(w/w_c\right)^n\right] \quad [4]$$

where n is the fitting parameter which he found to be between 0.2–0.4 for normal concrete [23].

The more recent studies of tension-softening of concrete[24], were still based on previously-described simplified models, although newer test set-ups were used together with improved crack-detection techniques such as digital image correlations. However, no improvements in understanding over the earlier simplified models have been reported.

Effects of the shape and the surface texture of aggregates

In concretes with rounded aggregate (e.g. river gravels), the macrocracks may coalesce by growing around the aggregate pieces. However, when rough/angular aggregate (e.g. crushed aggregate) are used, the macrocracks may follow the shortest path by growing through the aggregate pieces because of the high frictional resistances along tortuous crack paths. As a result, crushed aggregates give higher G_{Cl}. The simplified tension-softening models discussed above were based on results of concretes with crushed aggregates, and therefore, the models do not take account of the effects due to the shape and the surface texture of the aggregate.

The empirical model of Bažant and Becq-Giraudon[25], based on a large database of test results, takes account of these effects to predict G_{CI}. They quote (Eq. [5]):

$$G_{CI} = 2.5\,\alpha_0 \left(f_c'/0.051\right)^{0.46} \left(1 + d_{a\_max}/11.27\right)^{0.22} (W/C)^{-0.30} \qquad \text{(N, mm units)} \qquad [5]$$

where α_0 =1 and 1.44 for rounded and crushed aggregates respectively, and *W*/*C* is the water/cement ratio by weight of the mix.

Estimation of G_{CI}: An example

Table 1 shows the estimates for G_{CI} for a concrete mix with d_a of 0.8 in. (20 mm) (crushed aggregate) and W/C of 0.5 according to the bilinear models of Guinea et al.[22], and Gustafsson and Hillerborg[26]; and the polynomial model of Reinhardt[23]. The prediction from the empirical model is also shown in the table. The polynomial model gives a range of values to be expected from tests but does not give a method for predicting the exact value without doing tests. As shown in **Table 1**, the two bilinear models predict similar G_{CI} and they agree well with that from the polynomial model. The prediction from the empirical model also matches well with those from the simplified models but, as expected, the CEB–FIB model code expression[11] underestimates G_{CI}. The values quoted in the table suggests a value of 0.86 lbf/in. (0.15 N/mm) for the G_{CI} of the assumed concrete, which agrees with experimentally obtained G_{CI} for similar strength concretes with 0.8 in. (20 mm) crushed aggregates[16].

The incorporation of G_{CI} in the FRP debonding analysis gives predictions that match the test results reported in the literature[3]. The G_{CI} values used in that study were determined as below.

USE OF G_{CI} IN THE ANALYSES OF FRP DEBONDING

The global-energy-balance FRP debonding analysis was applied to several sets of beam tests reported in the literature[3]. The G_{CI} of the concretes used were not measured, so it is necessary

to decide on values that can be used in the analysis. The f_c' of the concretes used in the beams being tested were in the range 4–8 ksi (30–55 N/mm^2); crushed aggregates of 0.8 and 0.4 in. (20 and 10 mm) and 0.4 in. (10 mm) rounded aggregates were used in the mixes[3]. Since the f_c' of the beams did not vary significantly, it was assumed that variations in G_{CI} of these concretes mainly depend on the aggregate properties. **Table 2** shows the estimates for G_{CI} of the beams under consideration, calculated from data quoted by the experimenters, according to the simplified models and the empirical model discussed above. Since the softening models can only be used to estimate G_{CI} of concretes with crushed aggregates, the G_{CI} of the mixes with rounded aggregate were estimated using the empirical model only. When using the bilinear models, the coordinates of the kinking point (f_1, w_1 in **Fig. 8a**) were assumed to be $0.33f_t$ [22] and 0.001 in. (0.03 mm)[23] respectively, for all concretes. The values of f_t were obtained from Eq. [3]. The values for the w_{tip_c} of concretes with 0.4 and 0.8 in. (10 and 20 mm) crushed aggregates were assumed to be 0.005 and 0.007 in. (0.130 and 0.175 mm) respectively, based on the typical values recommended in the CEB–FIP model code[11].

Based on the values quoted in **Table 2**, the G_{CI} of mixes with crushed aggregates of 0.8 and 0.4 in. (20 and 10 mm) and 0.4 in. (10 mm) rounded aggregates were assumed to be 0.86, 0.57 and 0.40 lbf/in. (0.15, 0.10 and 0.07 N/mm) respectively. These values agree with experimentally-obtained G_{CI} values for concretes with similar properties[16]. The measured G_{CI} values were often associated with a scatter of about 10%, so to illustrate the significance of this variability, results for a ±10% variation in G_{CI} was considered in the debonding analysis[3].

Results of debonding analyses

All the beams analysed in the present study were tested as simply-supported beams under four-point bending with equal shear spans[3]. A large database of beam specimens, including a

variety of material and geometric properties, and also covering beams that failed in all possible modes of FRP debonding, was investigated. Comparisons made in this study[3] have shown that the assumption of these G_{CI} values in the analyses predicted results that match the experimental data. A single example for each of PE and IC debonding are shown below.

Example: Plate-end debonding

When the FRP is curtailed at a considerable distance away from the beam support, debonding is likely to initiate due to the formation of a dominant shear crack near to the plate end. Further extension of this crack forms an interface crack, so the effective plate end location (L_{0_e}), just prior to the initiation of rapid propagation of debonding, is now placed slightly away from the actual plate end (L_0) (**Fig. 9**). It was assumed that the original shear crack propagates along a direction at about 45° to the interface (the actual direction of propagation may be slightly varied from this, but it should not have a significant effect on the results predicted by the model), up to the level of tension-steel bars in the beam, and therefore, it was contended that L_{0_e} should be located between L_0 and a further cover distance (c) into the beam (**Fig. 9**). The energy release rates (G_R) associated with L_{0_e} values in the range L_0–2c and L_0+2c were determined and compared with G_{CI} (including a range with ±10% variation in G_{CI}) to decide whether debonding is possible at the reported failure load (P_f).

Fig. 10 shows the variation in G_R vs. L_{0_e} for beam pair F9 and F10 selected from the study of Fanning and Kelly[27] (L_0= 20 in. (500 mm) and c=1.2 in. (30 mm)). The G_{CI} of the concrete with 0.8 in. (20 mm) crushed aggregate was assumed to be 0.86 lbf/in. (0.15 N/mm). The figure shows that taking L_{0_e} to be 0.4 in. (10 mm) higher than the actual L_0 (i.e. $L_0<L_{0\_e}<L_0+c$), the failure load predicted from the model compares well with the P_f observed in the experiment. The figure also shows that, at the observed P_f any L_{0_e} shorter than the actual

L_0 could not cause PE debonding, since an interface crack of a positive magnitude is required to trigger failure. **Fig. 10** also shows that loads 10% higher or lower than P_f are too strong or too weak respectively to cause failure within the range between L_0 and L_0+c. Thus, the results of the present analyses match with the observed P_f and failure mode.

Example: Intermediate-crack-induced debonding

Earlier analyses by the authors[3] have shown that, in four-point bending beams, interface cracks formed due to widening of flexural cracks located at about a half beam depth (h) away from the loading point cause IC debonding (**Fig. 11**). Analyses of IC debonding observed in a set of beams (Group 1) reported in the study of Ross et al.[31] are discussed below.

Possible propagation of interface cracks that are assumed to initiate at the critical location (x_c) of the beam span (i.e. ½ h away from the loading point) and, a further ½ h and h towards the nearest beam end were investigated. A concrete with 0.4 in. (10 mm) crushed aggregate was used in the beams, so G_{C1} was assumed to be 0.57 lbf/in. (0.10 N/mm). The solid line in **Fig. 12a** shows the variation in G_R vs l_d (crack length) for an interface crack that initiates at x_c, at the observed P_f. The figure shows that l_d of 0.08 in. (2 mm) would cause failure here; it has been observed that widening of a critical flexural crack in the high moment zone forms interface cracks of this magnitude[29]. The dashed lines in **Fig. 12a** show that, if the debonding initiated at ½ h or h away towards the nearest beam end, much longer cracks of lengths 0.14 in. (3.5 mm) and 0.24 in. (6 mm) respectively, would be required to cause debonding at P_f; these are less likely to occur. The conditions needed for debonding to initiate at x_c at 90% of P_f is also investigated in **Fig. 12b**. The figure shows that a critical crack of length about twice that required at P_f would be required to cause failure here so again is less likely.

CONCLUSIONS

- The paper has shown that the FRP force, acts with an eccentricity with respect to the tip of the crack that triggers PE debonding, causes a dominant tension in the crack tip, and hence the crack starts to propagate by opening.
- In IC debonding, the FRP cannot slide parallel to the concrete because it is fixed at both ends of the unbonded zone, but it can move away from the surface.
- Thus, in both types of debonding, even though the interface of a strengthened beam, is primarily carrying shear, it actually fails in tension. Thus, debonding propagates locally as a Mode I fracture in concrete.
- Debonding occurs in a narrow zone of concrete, between the FRP and the internal steel bars of the beam, and therefore, a conventional fracture analysis of the fracture process zone, which is typically over 12 in. (300 mm) long, cannot be performed.
- It is appropriate to assume that the fracture energy to be used in a debonding analysis should be the value obtained from small-scale test specimens.
- Appropriate non-linear models to determine the Mode I fracture energy of concrete, to an accuracy that can be used in the analysis of FRP debonding, have been presented.
- The incorporation of the Mode I fracture energy of concrete in the FRP debonding analyses, gives predictions that match the experimental results reported in the literature.

NOTATION

d_a = maximum size of the aggregates used in the concrete mix

f_c', f_t = compressive and tensile strength of concrete respectively

G_C = fracture energy of concrete

G_{CI}, G_{CII} = Modes I and II fracture energy of concrete respectively

G_F , G_{F_int} = fracture energy and interface fracture energy respectively

G_R = energy release rate

w = width of the separation between the two surfaces of a crack

σ = stress

REFERENCES

1. Achintha, M., and Burgoyne, C. J., "Moment–Curvature and Strain Energy of Beams With External FRP Reinforcement," *ACI Structural Journal*, V. 106, No. 1, Jan-Feb. 2009, pp. 20-29.
2. Achintha, M., and Burgoyne, C. J., "Fracture Mechanics of Plate Debonding," *Journal of Composites for Construction*, V. 12, No. 4, 2008, pp. 396-404.
3. Achintha, M., and Burgoyne C. J., "Fracture Mechanics of Plate Debonding: Validation Against Experiments," *Construction and Building Materials*, doi: 10.1016/j.conbuildmat.2010.11.103.
4. Büyüköztürk, O.; Günes, O.; and Karaca, E., "Progress on Understanding Debonding Problems in Reinforced Concrete and Steel Members Strengthened Using FRP Composites," *Construction and Building Materials*, V. 18, No. 1, 2004, pp. 9-19.
5. Hutchinson, J. W., and Suo, Z., "Mixed Mode Cracking in Layered Materials," *Advances in Applied Mechanics*, V. 29, 1992, pp. 63-191.
6. Karihaloo, B.L., "*Fracture Mechanics and Structural Concrete*," Addison Wesley Longman Limited, England. 1995.
7. Kotsovs, M. D., and Pavlovic, A., "*Structural Concrete*," Thomas Telford Publications, London, 1995.
8. Wang, J.; and Zhang, C., "Nonlinear fracture mechanics of flexural-shear crack induced debonding of FRP strengthened concrete beams," *Int. J. Solid Struct.*, V. 45, No. 2, 2008, pp. 2916-2936.

9. Deric John Oehlers, D. J.; Mohamed-Ali M. S.; Matthew Haskett, M.; Lucas, W.; Muhamad, R.; and Visintin, P.; "FRP-Reinforced Concrete Beams: Unified Approach Based on IC Theory," V. 15, No. 3, 2011, pp. 293-303.
10. Branson, D. E., "Design Procedures for Computing Deflections," *ACI Journal Proceedings*, V. 65, No. 9, Sept. 1968, pp. 730-735.
11. Comite Euro-International du Beton-Federation Internationale de la Precontrainte, "CEB–FIP Model Code," Lausanne, Switzerland, 1991.
12. Gálvez, J. C.; Elices, M.; Guinea, G. V.; and Planas, J., "Mixed Mode Fracture of Concrete Under Proportional and Nonproportional Loading," *International Journal of Fracture*, V. 94, No. 3, 1998, pp. 267-284.
13. Subramaniam, K.V.; Carloni, C.; and Nobile, L., "Width Effect in the Interface Fracture During Debonding of FRP From Concrete," *Engineering Fracture Mechanics*, V. 74, No. 4, 2007, pp. 578-594.
14. Qiao, P., and Xu, Y., "Evaluation of Fracture Energy of Composite–Concrete Bonded Interfaces Using Three–Point Bend Tests," *Journal of Composites for Construction*, V. 8, No. 4, 2004, pp. 352-359.
15. Shah, S. P., and Ouyang, C., "Fracture Mechanics for Failure of Concrete," *Annual Review of Material Science*, V. 24, 1994, pp. 293-320.
16. Karihaloo, B. L.; Abdalla, H. M.; and Imjai, T., "A Simple Method for Determining the True Fracture Energies of Concrete," *Magazine of Concrete Research*, V. 55, No. 5, 2003, pp. 471-481.
17. Shah, S. P., and Carpinteri, A. (ed.), "*Fracture Mechanics Test Methods for Concrete – RILEM Report 5*," Chapman & Hall Publisher, London, 1991.

18. RILEM Committee 50-FMC, "Determination of the Fracture Energy of Mortar and Concrete by Means of the Three–Point Bend Tests on Notched Beams," *Materials and Structures*, V. 18, No. 4, 1985, pp. 287-290.
19. Hillerborg, A.; Modéer, M.; and Petersson, P. E.; "Analysis of Crack Formation and Crack Growth in Concrete by Means of Fracture Mechanics and Finite Elements," *Cement and Concrete Research*, V. 6, No. 6, 1976, pp. 773-782.
20. British Standards Institution, "Eurocode 2: Design of Concrete Structures. Part 1-1: General Rules and Rules for Buildings," London, 2004.
21. Raiss, M. E., "Observation of the Development of Fracture Process Zone in Concrete Under Tension," PhD Thesis, Imperial College, London, 1986.
22. Guinea, G. V.; Planas, J.; and Elices, M., "A General Bilinear Fit for the Softening Curve of Concrete," *Materials and Structures*, V. 27, No. 2, 1994, pp. 99-105.
23. Reinhardt, H. W., "Crack Softening Zone in Plain Concrete Under Static Loading," *Cement and Concrete Research*, V. 15, No. 1, 1985, pp. 42-52.
24. Barr, B., and Lee, M. K., "Modeling the Strain–Softening Behaviour of Plain Concrete Using a Double–Exponential Model," *Magazine of Concrete Research*, V. 55, No. 4, 2003, pp. 343-353.
25. Bažant, Z. P., and Becq-Giraudon, E., "Statistical Prediction of Fracture Parameters of Concrete and Implications for Choice of Testing Standard," *Cement and Concrete Research*, V. 32, No. 4, 2001, pp. 529-556.
26. Gustafsson, P. J, and Hillerborg, A., "Improvements in Concrete Design Achieved Through the Application of Fracture Mechanics," In Shah S. P. (ed.), *Application of Fracture Mechanics to Cementitious Composites*, Dordrecht, The Netherlands, 1985, pp. 639-680.

27. Fanning, P. J., and Kelly, O., "Ultimate Response of RC Beams Strengthened With CFRP Plates," *Journal of Composites for Construction*, V. 5, No. 2, 2001, pp. 122-127.
28. Nguyen, D. M., Chan, T. K., and Cheong, H. K., "Brittle Failure and Bond Development Length of CFRP–Concrete Beams," *J. Compos. Constr.*, V. 5, No. 1, 2001, pp. 12-17.
29. Garden, H. N.; Quantrill, R. J.; Hollaway, L. C.; Thorne, A.M.; and Parke, G. A. R., "An Experimental Study of the Anchorage Length of Carbon Fibre Composite Plates Used Strengthened Reinforced Concrete Beams," *Construction and Building Materials*, V. 12, No. 4, 1998, pp. 203-219.
30. Jones, R., Swamy, R. N., and Charif, A., "Plate Separation and Anchorage of Reinforced Concrete Beams Strengthened by Epoxy–Bonded Steel plates," *The Structural Engineer*, V. 66, No. 5, 1988, pp. 85-94.
31. Ross, C. A.; Jerome, D. M.; Tedesco, J. W.; and Hughes, M. L., "Strengthening of Reinforced Concrete Beams With Externally Bonded Composite Laminates," *ACI Structural Journal*, V. 96, No. 2, Mar-April. 1999, pp. 212-220.
32. Arduini, M., Di Tommaso, A., and Nanni, A., "Brittle Failure in FRP Plate and Sheet Bonded Beams," *ACI Struct. J.*, V. 94, No. 4, 1997, pp. 363-370.
33. Quantrill, R. J., Hollaway, L. C., and Thorne, A. M., "Experimental and analytical Investigation of FRP Strengthened Beam Response: Part I". *Mag. Concrete Res.*, V. 48, No. 4, 1996, pp. 331-342.

TABLES AND FIGURES

List of Tables:

List of Figures:

Table 1– Estimation of G_{CI} of the assumed concrete mix

Reference	Model	G_{CI}, lb_F/in. (N/mm)
Gustafsson and Hillerborg [26]	bilinear softening	0.799 (0.140)
Reinhardt [23]	power relation	0.474–0.811 (0.083–0.142)
Guinea et al. [22]	bilinear softening	0.828 (0.145)
Bažant and Becq-Giraudon [25]	empirical	0.640 ± 0.194 (0.112 ± 0.034)
CEB–FIP model code [11]	empirical	0.471 ± 0.143 (0.0825 ± 0.025)

Table 2– Estimation of G_{CI} of studied concrete beams

Aggregate Type	Reference	G_{CI}, lb_F/in. (N/mm)				
		Estimates from the models				Assumed G_{CI} for debonding analysis
		Bilinear models		Polynomial model	Empirical model	
		Gustafsson & Hillerborg	Guinea et al.	Reinhardt	Bažant & Becq-Giraudon	
20 mm Crushed	Fanning & Kelly [27]	1.028 (0.18)	0.971 (0.17)	0.685– 1.199 (0.12–0.21)	0.742 (0.13)	0.857 (0.15)
	Nguyen et al. [28]	0.857 (0.15)	0.799 (0.14)	0.571– 1.028 (0.10–0.18)	0.685 (0.12)	
	Garden et al. (Beam $1_{U,4.5}$) [29]	0.857 (0.15)	0.799 (0.14)	0.571– 1.028 (0.10–0.18)	0.685 (0.12)	
10 mm Crushed	Jones et al. [30]	0.685 (0.12)	0.571 (0.10)	0.457– 0.628 (0.08–0.11)	0.571 (0.10)	0.571 (0.10)
	Ross et al. [31]	0.742 (0.13)	0.628 (0.11)	0.514– 0.742 (0.09–0.13)	0.628 (0.11)	
	Garden et al. (Beam $3_{U,1.0}$) [29]	0.685 (0.12)	0.571 (0.10)	0.457– 0.628 (0.08–0.11)	0.571 (0.10)	
10 mm Rounded	Arduini et al. [32]	N/A	N/A	N/A	0.388 (0.068)	0.40 (0.07)
	Quantrill et al. [33]	N/A	N/A	N/A	0.417 (0.073)	

N/A – not applicable

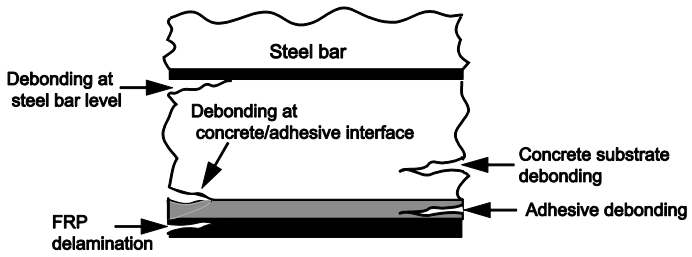

Fig. 1. Possible phases for the initiation of the dominant interface crack

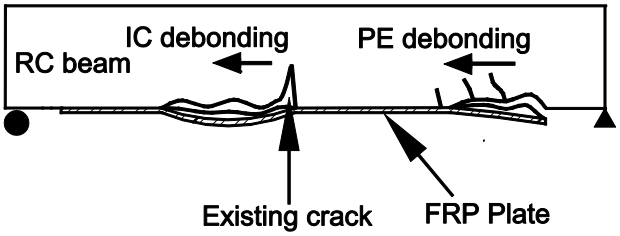

Fig. 2. Two modes of debonding

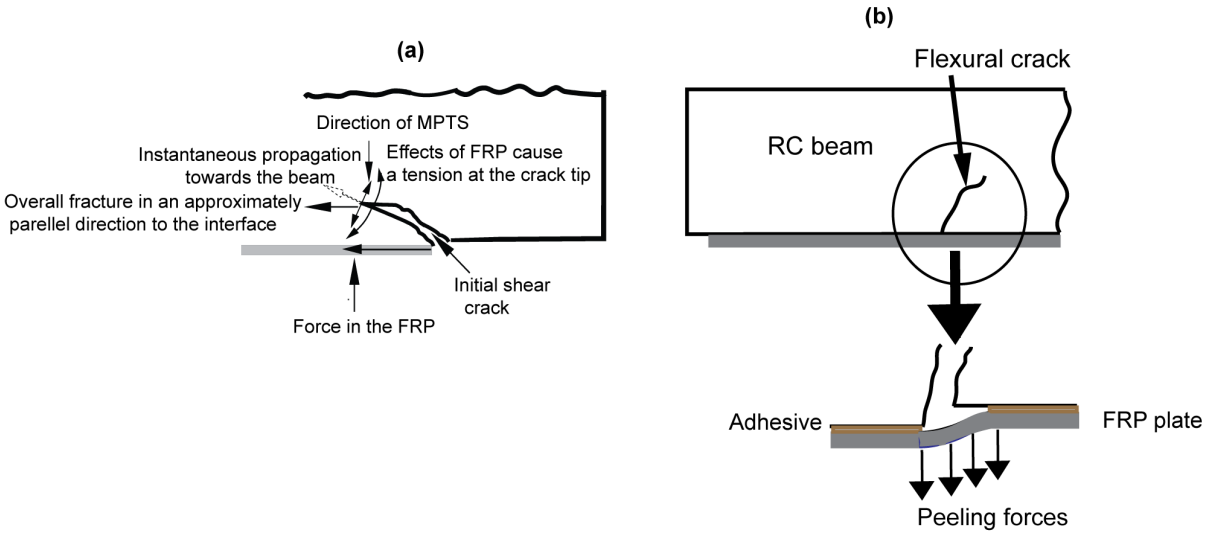

Fig. 3. (a) Effect of the FRP causes a significant tension at the tip of the shear crack during PE debonding

(b) Relative sliding between the two faces of flexural cracks causes interface flaws that trigger IC debonding

1

2

3

4

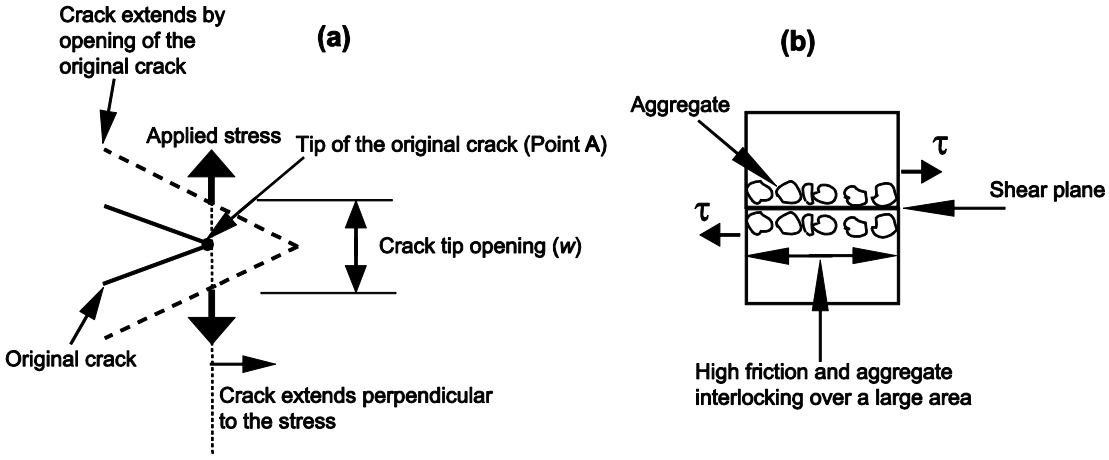

Fig. 4 – (a) Mode I crack propagation (b) High fracture resistance against a shear crack

5

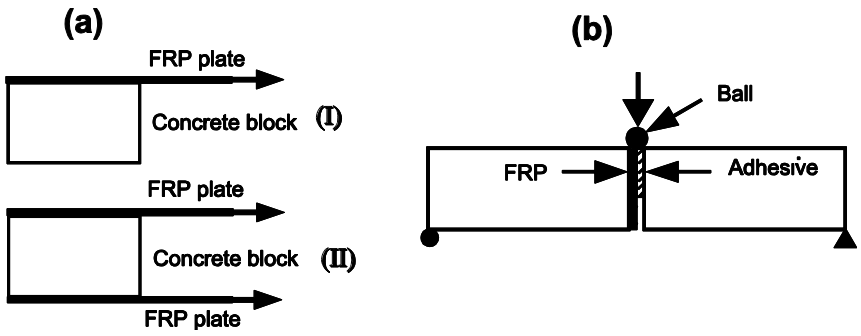

Fig. 5. – (a) **(**I) - single (II) - double shear lap specimens (b) A modified three-point bend specimen

1

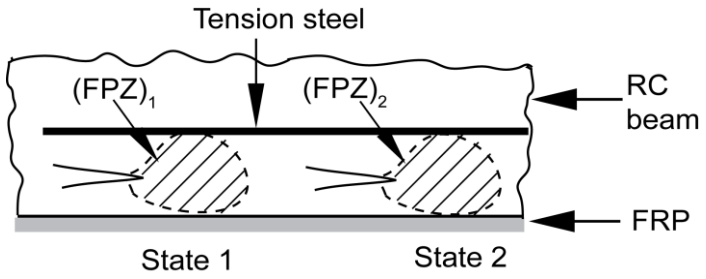

Fig. 6. – Crack before and after extension

2

3

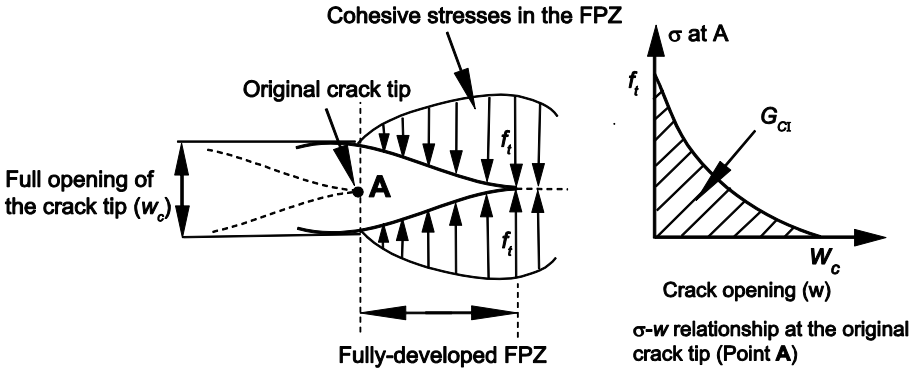

Fig. 7. – Cohesive crack model (Hillerborg et al. [19])

4

5

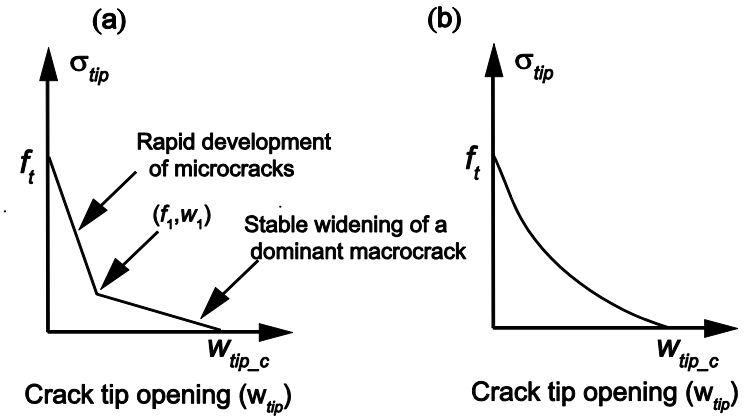

Fig. 8. – Simplified tension-softening models (a) bilinear (b) polynomial

1

2

3

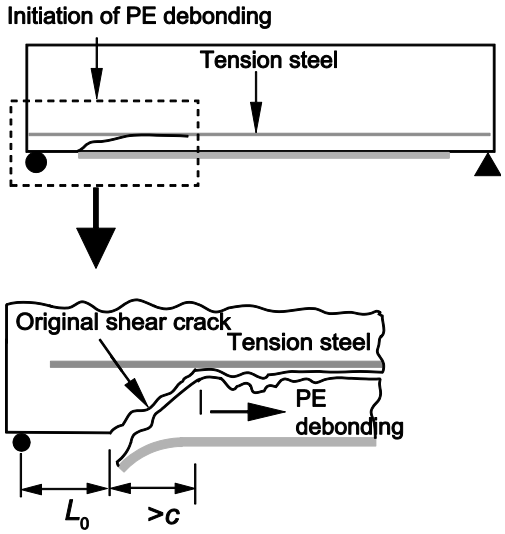

Fig. 9 – Location of the effective plate end

4

5

6

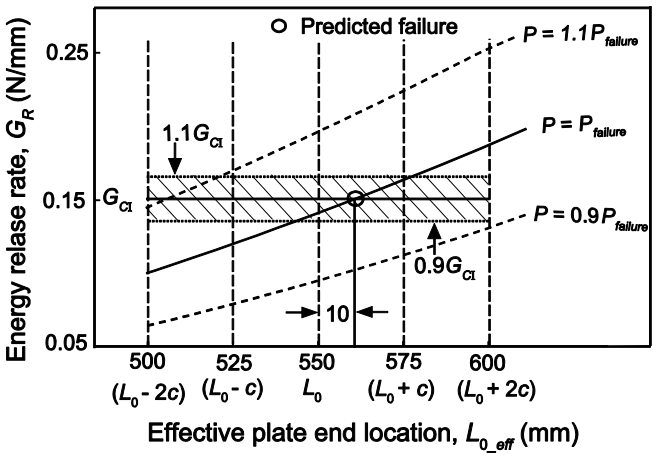

Fig. 10 – G_R vs L_{0_eff} plots for beam set F9 and F10 (Fanning and Kelly [27])

(Note: 1 N/mm = 5.71 lb_F/in.; 1 mm = 0.0393 in.)

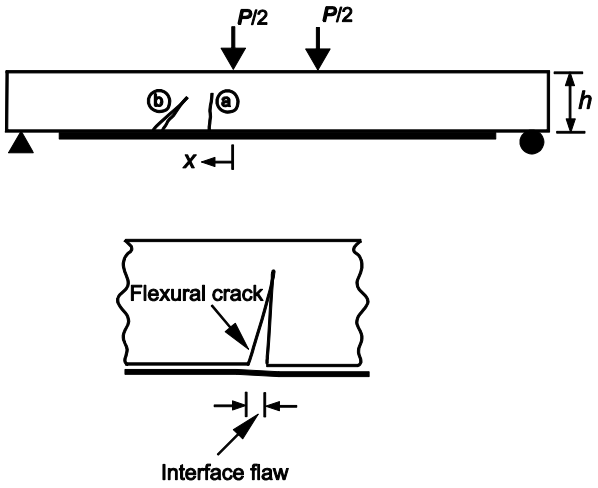

Fig. 11 – Initiation of IC debonding by widening of flexural cracks

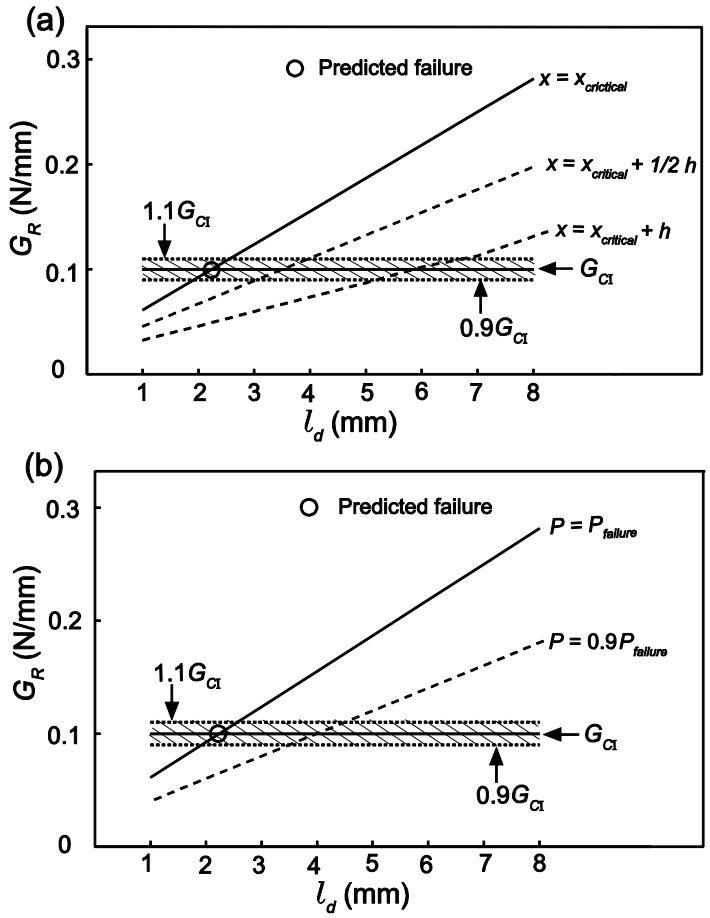

Fig. 12 – G_R vs l_d plot for Group 1 beam (Ross et al. [31]) for fractures starting at (a) different locations (b) 90% of the failure load

(Note: 1 N/mm = 5.71 lb_F/in.; 1 mm = 0.0393 in.)